Evaluation of rock brittleness based on the ratio of stress drop rate to strain drop rate and peak strength

Chenyang Liu, Xiaopei Zhang*, Lizhi Du, Yong Wang, Bingbing Chen, Jie Wang

College of Construction and Engineering, Jilin University, Changchun 130012, China

xiaopei@jlu.edu.cn

ABSTRACT. This paper aims to overcome the imitations of the existing indices in the evaluation of rock brittleness. Considering the importance of brittleness evaluation in rock engineering, this paper analyses the existing brittleness indices against brittleness features like strength, stress-strain curve, hardness, mineral composition, internal friction angle, elastic modulus, Poisson's ratio, etc., revealing that each approach has its strengths and weaknesses. For instance, the index of rupture angle is too difficult to identify accurately, while the indices based on stress-strain curve are easy to obtain and quantify. On this basis, a new brittleness index (B_L) was proposed based on the ratio of stress drop rate to strain drop rate (drop rate ratio0 and the peak strength. Then, the proposed index was validated through uniaxial and triaxial compression tests, and compared with B_8, B_{11} and B_{12}. It is concluded that the proposed index could accurately identify rock brittleness under different confining pressures, and outperform other indices in revealing the variation of rock brittleness; the index could also accurately reflect the brittle anomalies of the rock specimen at the confining pressure of 15MPa, making it a desirable tool to evaluate rock brittleness under uniaxial compression.

RÉSUMÉ. Cet article vise à surmonter les imitations des indices existants dans l'évaluation de la fragilité des roches. Considérant l'importance de l'évaluation de la fragilité dans l'ingénierie des roches, cet article analyse les indices de fragilité existants par rapport à des caractéristiques de fragilité telles que la résistance, l'essai de traction, la dureté, la composition minérale, l'angle de frottement interne, le module d'élasticité, le coefficient de Poisson, etc., qui révèle que chaque approche a ses forces et ses faiblesses. Par exemple, il est trop difficile d'identifier avec précision l'indice de l'angle de fracture, tandis que les indices basés sur l l'essai de traction sont faciles à obtenir et à quantifier. Sur cette base, un nouvel indice de fragilité (B_L) a été proposé en basant sur le ratio de la fréquence de chute de pression par rapport à la chute de vitesse de déformation et la force maximale. Ensuite, l'indice proposé a été validé par des tests de compression uniaxiale et triaxiale, et comparé avec B_8, B_{11} et B_{12}. Il est conclu que l'indice proposé pourrait identifier précisément la fragilité des roches sous différentes pressions de confinement et surpasser les autres indices en révélant la variation de la fragilité des roches; l'indice pourrait également refléter avec précision les anomalies fragiles

de l'échantillon de roche à la pression de confinement de 15 MPa, ce qui en fait un outil désirable pour évaluer la fragilité de la roche sous compression uniaxiale.

1. Introduction

Brittleness, a basic parameter of rock mechanics, plays a crucial role in rock failure engineering. On the one hand, this parameter measures the probability of rock burst, a major problem in underground excavation like tunnel engineering (Gong and Zhao, 2007; Yarali and Kahraman, 2011; Zhao *et al.*, 2015; Özfırat *et al.*, 2016); on the other hand, rock brittleness directly bears on the efficiency of the tunnel boring machine (Dursun and Gokay, 2016). In the energy field, brittleness determines the hydraulic fracturing effect of horizontal wells, thereby affecting the productivity of shale gas or oil (Holt *et al.*, 2015; Dursun and Gokay, 2016; Özfırat *et al.*, 2016). Hence, the accurate evaluation of rock brittleness is of great significance to the disaster prevention and mitigation for underground operations and the efficient exploitation of geological resources.

Despite its apparent importance, brittleness has been given various definitions and measuring methods. Morley and Hetényi (El-Ebrashi *et al.*, 1969) associated brittleness with low percent elongation or strain and defined it as the lack or excess of ductility. Ramsay (1967) considered brittleness as the loss of internal cohesion of elastically deformed rock under the peak stress specified in the strength criteria of brittleness. Similarly, Obert and Duvall (1967) regarded brittleness as the fracturing of materials (e.g. cast iron and rock) at or slightly beyond the yield stress. Tarasov and Potvin (2013) held that brittleness is the resistance to macroscopic failure in the post-peak area under the compressive load curve of cumulative elastic energy.

Of course, there is an agreement on the definition of brittleness among quite a few scholars (Hucka and Das, 1974; Hajiabdolmajid and Kaiser, 2003; Kahraman and Altindag, 2004; Nygård *et al.*, 2006; Yagiz, 2009; Lee *et al.*, 2012; Liu and Sun, 2015). By the common definition, a brittle material has the following features: (1) fresh fractured surfaces in brittle failure; (2) grains and cracks in indentation; (3) automatic crack propagation in failure process; (4) more prone to tensile failure than crack failure; (5) low strain deformation of grains under load; (6) high stress drop of post-peak curve; (7) abrupt release of elastic energy in failure process; (8) high resilience, i.e. high Young's modulus and low Poisson's ratio (Rickman, Mullen *et al.*, 2008); (9) big internal friction angle; (10) high brittle-ductile material ratio (e.g. proportion of quartz and clay). The popular brittleness evaluation methods and indices are listed in Table 1 below.

Table 1. Summary of commonly used rock brittleness indexes based on Class I stress-strain curves

Experiment methods	Formula meaning and explanation
Based on the rock stress-strain curve	$B_1 = \sigma_c/\sigma_t$, $B_2 = (\sigma_c - \sigma_t)/(\sigma_c + \sigma_t)$, $B_3 = \sigma_c\sigma_t/2$, $B_4 = \sqrt{B_3}$, σ_c and σ_t are the UCS and the tensile strength, respectively.
	$B_5 = B_5'B_5''$, $B_5' = (\varepsilon_{BRIT} - \varepsilon_n)/(\varepsilon_m - \varepsilon_n)$, $B_5'' = \alpha CS + \beta CS + \eta$, $CS = \varepsilon_p(\sigma_p - \sigma_r)/\sigma_p/(\varepsilon_r - \varepsilon_p)$, ε_{BRIT}, ε_m, ε_n are the peak strain, the peak strain maximum and the minimum value of sample rock specimen, respectively. α, β, η are the standardized coefficients. σ_p and σ_r are the peak strength and the residual strength, respectively. ε_p and ε_r are the peak strain and the residual strain, respectively.
	$B_6 = (M - E)/M$, $B_7 = E/M$, M and E are the post-peak modulus and the pro-peak elastic modulus, respectively.
	$B_8 = (\sigma_p - \sigma_r)/\sigma_p$, $B_9 = (\varepsilon_r - \varepsilon_p)/\varepsilon_p$, $B_{10} = \varepsilon_R/\varepsilon_P$, σ_p and σ_r are the peak strength and the residual strength, respectively. ε_r and ε_P are the peak strain and the residual strain, respectively, ε_R is the reversible strain of the stress-strain curve.
	$B_{11} = B_{11}'B_{11}''$, $B_{11}' = (\sigma_p - \sigma_r)/\sigma_p$, $B_{11}'' = \lg\|k_{ac}\|/10$, σ_p and σ_r are the peak strength and the residual strength, respectively. k_{ac} is the post-peak stress drop rate.
	$B_{12} = B_{12}' + B_{12}''$, $B_{12}' = (\sigma_p - \sigma_r)/(\varepsilon_r - \varepsilon_p)$, $B_{12}'' = (\sigma_p - \sigma_r)(\varepsilon_r - \varepsilon_p)/(\sigma_p\varepsilon_p)$, σ_p and σ_r are the peak strength and the residual strength, respectively.
Based on the inner friction angle	$B_{13} = \sin\beta$, $B_{14} = 45° + \beta/2$, β is the inner friction angle determined from Mohr's envelope.
Based on the elastic modulus and Poisson's ratio	$B_{15} = 0.5E_{brit} + 0.5\mu_{brit}$, $E_{brit} = (E - 1)/(8 - 1) \times 100$, $\mu_{brit} = (0.4 - 1)/(0.4 - 0.15)$, E and μ are the post-peak modulus and the elastic modulus, respectively.
Based on the hardness	$B_{16} = (H_\mu - H_m)/c$, where Hμ is the micro-indentation hardness, Hm is the macro-indentation hardness, and c is the constant $B_{17} = H_a/K_c$ where Ha is hardness and Kc is fracture toughness. $B_{18} = H_aE/K_c^2$ where Ha and Kc are same as those in B16, E is Young's modulus.
Based on the mineral composition	$B_{19} = W_{qtz}/(W_{qtz} + W_{carb} + W_{clay})$, Wqtz, Wcarb and Wclay are the content of quartz, clay and carbonate minerals, respectively.

1.1. Indices based on rock stress-strain curve

In Table 1, indices $B_1 \sim B_4$ are based on the relationship between uniaxial compressive strength (UCS) and tensile strength. Among them, B_1 was proposed by George based on experimental results. Kahraman (2002) discovered the strong exponential correlations between the penetration rate of rotary drill and indices B_1 and B_2. According to the tensile-compressive strength curve, Altindag (2002) quantified rock brittleness with indices B_3 and B_4, and applied the brittleness to accurately predict rock drillability. However, $B_1 \sim B_4$ are not suitable for analysing rock brittleness under complex stress states (Bishop, 1967; Meng *et al.*, 2015; Bai, 2016).

The index B_5 was put forward based on the modality index of post-peak curve and peak strength by Jim Liang *et al.* (Qing *et al.*, 2012) through an experiment on the black shale specimens from southern China. Nevertheless, it is impractical to use this index in engineering or compare it with other indices, for repeated experiments are needed to obtain the accurate parameters of even one type of rock.

Meanwhile, Tarasov and Potvin (2012) presented new brittleness indices B_6 and B_7 based on post-peak secant modulus and pre-peak elastic modulus, respectively. Nevertheless, Xia *et al.* suggested that these indices cannot effectively distinguish between the brittleness of different stress-strain curves.

Considering peak and residual stress-strains, Bishop (1967), Hucka and Das (1974) invented indices $B_8 \sim B_{10}$, which involve too few parameters to reflect the generation of the stress-strain curve of rock. Thus, the accuracy of these three indices should be re-examined.

Meng *et al.* created the brittleness index B_{11} based on the relative magnitude and absolute velocity of post-peak stress drop and verified it by comparing various types of rock under different levels of confining pressure. Nonetheless, Xia *et al.* argued that this parameter does not apply to the case of equal drop rate of post-peak stress, and that the mechanical features vary across the peaks on the stress-strain curves.

Xia *et al.* introduced B_{12} to reflect the post-peak stress drop rate and the ratio of the elastic energy released in failure to the total energy accumulated before the peak strength (hereinafter referred to as the elastic-total energy ratio), and verified the feasibility of the index through a brittleness test on rock mass under different confining pressures. On the upside, this index, considering the effects of both stress and strain, is more reasonable than the previous ones; on the downside, B_{12} does not take account of the main features of brittle failure.

Figure 1 illustrates a case that cannot be accurately described by B_{12}. In this figure, OAC and OBD are the stress-strain curves of two rock masses sharing the same post-peak stress drop rate and the same elastic-total energy ratio. It can be empirically concluded that the rock will shift from brittle state to ductile state with the increase of the confining pressure, leading to a growth of the peak stress. Thus, the rock mass described by OBD must be less brittle than that by OAC. However, this relationship cannot be revealed by B_{12}.
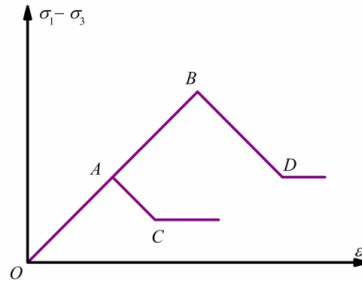
Figure 1. A case that cannot be accurately described by B_{12}

1.2. Indices based on internal friction angle

Using the internal friction angle, Hucka and Das (1974) proposed brittleness indices B_{13} and B_{14} to quantify the rock brittleness. Tarasov and Potvin (2013) discovered the positive correlation between B_{13} and rock rupture angle through experiments. Nonetheless, these two indices can only identify the brittleness of a few types of rock, and their identification effect is severely constrained by the difficulty in acquiring accurate rock fracture angles.

1.3. Index based on elastic modulus and Poisson's ratio

Rickman, Mullen *et al.* (2008) came up with B_{15} for the shale reservoir in Fort Worth Basin, US, considering both elastic modulus and Poisson's ratio. However, this index is featured by low adaptability and poor accuracy, as it ignores many important parameters, such as residual strength, peak strength and residual strain, and requires too many specimens and resources to obtain accurate parameters.

1.4. Indices based on hardness

Hucka and Das proposed B_{16} is proposed (1974) in view of the difference between hardness and micro-indentation. Lawn and Marshall (1979) established B_{17} in ceramic engineering, with H_a being the hardness of the ceramic and K_c being the fracture toughness. Quinn and Quinn (1997) developed B_{18} to measure rock brittleness based on the ratio of the deformation energy per unit volume to the rupture surface energy per unit area. The applicability of these hardness-based indices to materials other than ceramics should be further investigated.

1.5. Indices based on mineral composition

Miskimins (2012) used B_{19} to evaluate the brittleness of shale, a common rock in shale gas mining. Solely based on mineral composition, this index overlooks the

impacts of stress state and diagenesis on the rock brittleness. As mentioned before, the rock will shift from brittle state to ductile state with the increase of the confining pressure, leading to a growth of the peak stress. Besides, the rocks formed in different geological periods must differ in structure, compactness, porosity, and thus brittleness. All these conditions severely limit the applicable range of B_{19}.

1.6. Discussion on the evaluation method of rock brittleness

All the above indices require numerous parameters and face severe limitations in the evaluation of rock brittleness. To solve the problems, this paper puts forward a new index B_L based on the ratio of stress drop rate to strain drop rate (hereinafter referred to as the drop rate ratio) and the peak strength. Then, the index was verified through an experiment on phyllite rock specimens obtained from a deep tunnel in southwestern China. The results show that the index reflects the degree of difficulty for brittleness failure, and the exact variation of brittleness under uniaxial and confining pressures.

2. Rock brittleness indices based on drop rate ratio and peak strain

The current evaluation methods for rock brittleness in hydraulic fracturing generally take account of only a few mechanical parameters. For example, $B_1 \sim B_4$ only considers the stress variation, while $B_5 \sim B_6$ fail to explain the entire failure process. What is worse, the existing indices only apply to the uniaxial loading condition, but not the triaxial loading condition, in which deep tunnel projects face high confining pressure.
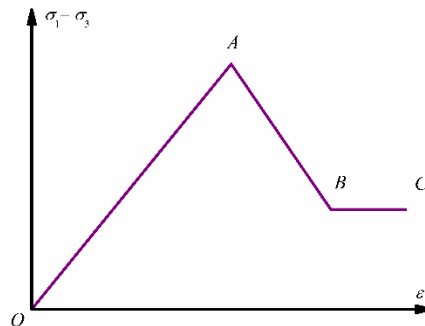

Figure 2. Stress-strain curve for B_L

To solve the defects of the current methods, several features were summarized for our new index on rock brittleness: (1) the impacts of confining pressure, e.g. the effect of uniaxial stress, must be took into consideration; (2) more mechanical parameters should be included to make the brittleness evaluation more comprehensive; (3) the

said parameters should be obtained accurately and easily.

The quantitative brittle parameters were obtained by the stress-strain curve, which reflects the entire failure process of rock mass. After all, the shape of the post-peak stress-strain curve obtained through lab experiment is the main way to identify the rock brittleness in a qualitative manner (Meng, Zhou *et al.*, 2015). Finally, a new brittleness index B_L was proposed based on the drop rate ratio obtained from post-peak stress-strain curve and the peak strength.

In Figure 2, the polyline ABC is a simplified Class I stress-strain curve; $A\ (\sigma_p, \varepsilon_p)$ is the peak point, with σ_P and ε_P being the peak strength and the peak strain, respectively; $B\ (\sigma_r, \varepsilon_r)$ is the residual point, with σ_r and ε_r being the residual strength and the residual strain, respectively. Divided into three segments by the two points, the polyline can be expressed in a quantitative manner.

As mentioned before, the new brittleness index B_{L1} was developed from the drop rate ratio, aiming to overcome the problems of the existing indices. To highlight the increase of post peak strain, the peak strain on the denominator of B_{L1} was replaced by the residual strain.

Thus, the new index can be expressed as:

$$B_{L1} = \frac{\sigma_p - \sigma_r}{\sigma_p} \cdot \frac{\varepsilon_r}{\varepsilon_r - \varepsilon_p}$$

where ε_r and ε_p are the peak strain and the residual strain, respectively; σ_p and σ_r are the peak strength and the residual strength, respectively. The peak strain demonstrates the difficulty of brittle failure (Meng *et al.*, 2015). Since the rock shifts from brittle state to ductile state with the increase of the peak pressure, the reciprocal of the peak strain B_{L2} was solved to express the difficulty of brittleness failure:

$$B_{L2} = \frac{1}{\varepsilon_P}$$

Based on B_{L1} and B_{L2}, the new rock brittleness evaluation method B_L can be obtained:

$$B_L = B_{L1} \times B_{L2}$$

Hence, the rock brittleness index B_L not only considers the effect of post-peak stress-strain drop, but also the difficulty of brittle failure. In this way, it can accurately reflect the entire stress-strain process.

3. Experimental validation

This section explores the variation of rock brittleness with the change in confining pressure, a major influencing factor of rock brittleness.

3.1. Specimen preparation and experimental conditions

Table 2. Results of the triaxial compression tests

Confining	0	3	9	12	15	18	25
$\sigma_p(\times 10^2\,\text{MPa})$	0.419	0.467	0.586	0.605	0.658	0.7956	0.982
$\varepsilon_p(\times 10^{-3})$	2.59	2.71	3.39	3.63	3.84	4.51	5
$\sigma_r(\times 10^2\,\text{MPa})$	0.268	0.363	0.484	0.357	0.563	0.677	0.8085
$\varepsilon_r(\times 10^{-3})$	3.47	4.23	4.5	4.9	5.26	6.12	7.79
$\varepsilon_R(\times 10^{-3})$	1.656	2.106	2.799	2.142	3.286	3.837	4.117
Rupture angle (°)	85	79	75	70	70	65	60
B_6	0.037	-1.549	-0.908	0.080	-1.793	-1.657	-2.292
B_7	0.963	2.549	1.908	0.920	2.793	2.657	3.292
B_8	0.361	0.223	0.174	0.410	0.144	0.149	0.177
B_9	0.340	0.561	0.3274	0.350	0.370	0.357	0.558
B_{10}	0.639	0.777	0.826	0.590	0.856	0.851	0.823
B_{11}	0.081	0.041	0.034	0.094	0.026	0.028	0.032
B_{12}	0.294	0.194	0.149	0.339	0.120	0.127	0.161
B_{13}	0.996	0.982	0.966	0.939	0.939	0.906	0.866
B_L	0.549	0.229	0.208	0.436	0.139	0.126	0.099

Several phyllite specimens were obtained from a deep tunnel in southwestern China, processed into cylinders of 5cm in diameter and 10cm in height, and subjected to traditional triaxial compression tests to verify the accuracy of B_L. The tests were conducted on MTS815 rock testing system at different confining pressures. Considering the depth and lithology of specimens, the confining pressures were set to 0, 3, 9, 12, 15, 18 and 25MPa. During the tests, the sensor collected the axial and radial deformations and transmitted the data to a computer. The confining pressure was applied at 0.1MPa/s and held constant after reaching the pre-set values. The axial load was applied at 0.002mm/s in the displacement control mode. The results of the triaxial compression tests are listed in Table 2.

3.2. Verification of the proposed evaluation index

During the experiment, the data on load and deformation were collected and stored in the data acquisition system. Figure 3 presents the failure and stress-strain curve of the specimens.

Figure 3 presents the failure features of specimens at different confining pressures. It can be seen that the macro fractures of phyllite were mostly the shear-sliding failures on the surface of the schistosity structure, as well as the cross-cutting and composite sliding failures of the schistosity planes. With the increase of the confining pressure, the rupture angle and the failure surface roughness exhibited a deep decline and the specimens differed in damage patterns. Meanwhile, the rocks shifted from brittle state to ductile state. These phenomena indicate that the brittleness index is negatively correlated with the confining pressure. Moreover, the specimen under 12MPa confining pressure had a coarse fracture surface, due to the cracking induced by the confining pressure. Based on the data in Table 2, the brittleness indices B_L and $B_6 \sim B_{13}$ were calculated and plotted as Figure 4.
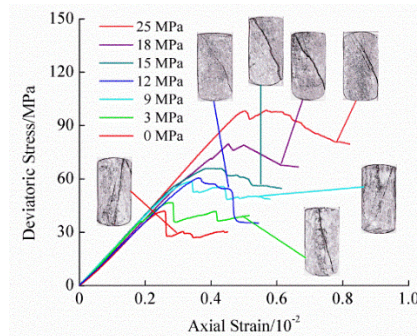

Figure 3. Failure features of specimens at different confining pressures

As shown in Figure 4, B_8, B_{11}, B_{12} and B_L carried the two necessary features of brittleness index, namely, reflecting the cracks under 12MPa and decreasing with the growth in confining pressure. The performances of the other indices are analysed in

details below.

The index B_6 revealed the anomalies caused by internal defects of the specimen under 12MPa, but failed to demonstrate the shift from brittle state to ductile state. This is because B_6 only tackles pre- and post-peak elastic modulus, without considering many relevant parameters.

The index B_7, which also only considers pre- and post-peak elastic modulus, could not reflect the trend of rock brittleness under different confining pressures.

The index B_9 did not reveal the brittleness variation with confining pressures, because it emphasises the effect of strain state over strength, residual strain and other associated parameters. To solve the problem, the residual strain of the denominator should be replaced by the peak strain.

The index B_{10} also failed to manifest the shift from brittle state to ductile state. The failure is attributable to the overlook of the effect of post-peak stress. This index merely takes account of the effect of the pre-peak recoverable strain and the peak strain on the brittleness evaluation.

The index B_{13}, focusing on the impact of the rupture angle, showed the negative correlation between brittleness and confining pressure, but ignored the brittleness anomalies caused by internal defects of the specimen at 12MPa. This is resulted from the neglection of stress drop rate, the strain drop rate, the residual strain factor, the difficulty of brittle failure, etc. The performance of this index is limited by the difficulty in accurate determination of fracture angles.
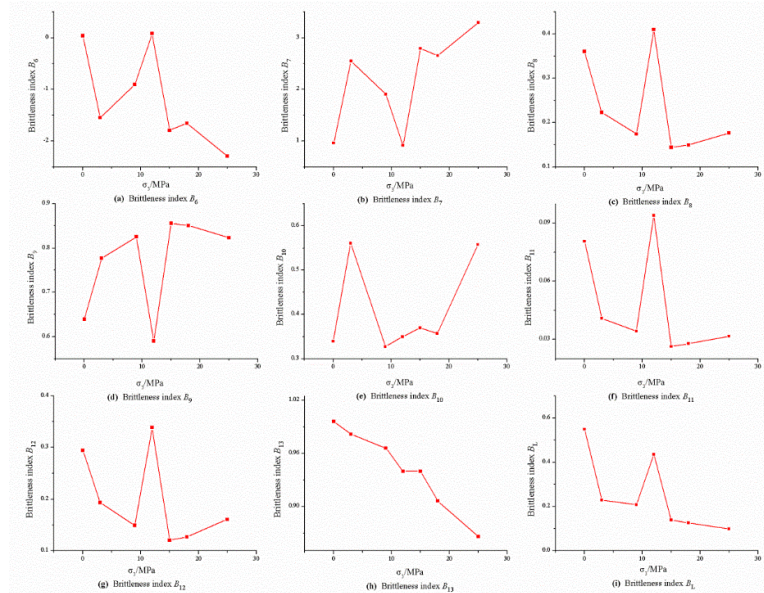

Figure 4. Brittleness index curves of the specimens under different confining pressures

To sum up, B_8, B_{11}, B_{12} and B_L accurately depicted the negative correlation between brittleness and confining pressure, which agrees well with the experimental data, and reflected the brittleness anomalies caused by internal defects of the specimen at 12MPa.

3.3. Further comparison

This subsection further compares B_8, B_{11}, B_{12} and B_L against the rupture features of specimens at 0~12MPa and 12~25MPa.

3.3.1. Rupture features at 0~12MPa

<div align="center">
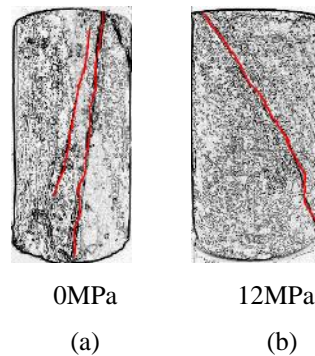
0MPa   12MPa

(a)   (b)

Figure 5. Results of the two specimens

</div>

The experimental results of the specimens at 0MPa and 12MPa are shown in Figure 5, where the red lines are the rupture surfaces. It is clear that the fracture angle was greater at 0MPa than 12MPa, while the rupture surface of specimen a was rougher than that of specimen b. Hence, specimen a has a greater brittleness index than specimen b. This is consistent with the experimental results. By contrast, the B_8, B_{11} and B_{12} values of specimen a were lower than those of specimen b, which goes against the experimental results.

3.3.2. Rupture features at 15~25MPa

Figure 6 presents the experimental results of the rock specimens at 15~25MPa, where the red lines are the rupture surfaces. As shown in this figure, the fracture angles of the three specimens were 70°, 65° and 60°, respectively.

The previous analysis points out that the brittleness index, fracture surface roughness and fracture surface penetration should decrease with the growth in confining pressure. It can be seen from Figure 6 that the rupture surface penetrated specimen c, but not specimens d and e, indicating that the brittleness is negatively correlated with the confining pressure. Therefore, B_L is more accurate than B_8, B_{11} and B_{12}, offering an effective supplement to the latter.

15 MPa   18 MPa   25 MPa
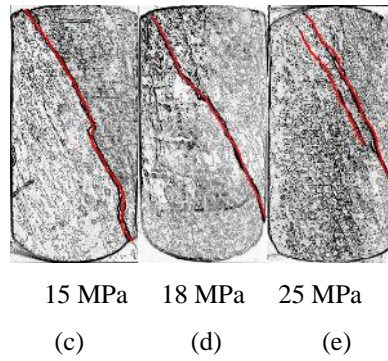
(c)   (d)   (e)

Figure 6. Results of the three specimens

4. Further validation

This section further validates the accuracy and adaptability of B_L against the existing experimental results (Tables 3 and 4).

Table 3. Mechanical parameters and brittleness indices B_{12} and B_L under different confining pressures

Confining pressure	$\sigma_p(\times 10^2 MPa)$	$\varepsilon_p(\times 10^{-3})$	$\sigma_r(\times 10^2 MPa)$	B_{12}	B_L
0	1.082	7.321	0.307	0.569	0.427
5	1.353	9.084	0.651	0.466	0.318
15	1.668	10.351	0.814	0.407	0.125
20	1.733	10.765	1.073	0.343	0.089
30	1.814	14.991	1.294	0.217	0.103
0	0.574	7.803	0.204	0.42	0.240
5	0.75	7.904	0.355	0.395	0.180
15	1.133	9.602	0.602	0.425	0.336
20	1.212	11.507	0.83	0.208	0.098
30	1.44	12.751	1.208	0.115	0.039

Table 4. Mechanical parameters and brittleness indices B_{12} and B_L under uniaxial compression

Simple no.	σ_p($\times 10^2 \text{MPa}$)	ε_p($\times 10^{-3}$)	σ_r($\times 10^2 \text{MPa}$)	ε_r($\times 10^{-3}$)	B_{12}	B_L
1	0.574	7.803	0.204	11.904	0.42	0.240
2	0.792	6.238	0.095	8.103	0.509	0.313
3	1.082	7.321	0.307	9.5	0.569	0.427
4	1.394	7.873	0.262	9.743	0.798	0.537

4.1. Further validation of B_L under different confining pressures

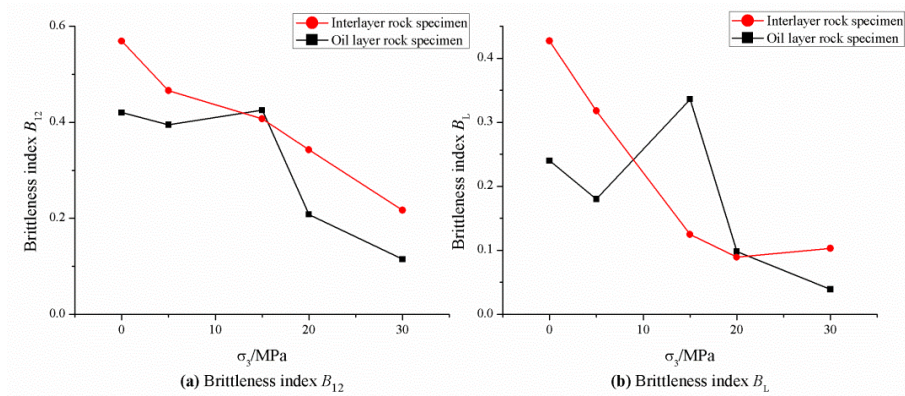(a) Brittleness index B_{12} (b) Brittleness index B_L

Figure 7. B_{12} and B_L under different confining pressures

The variation in B_{12} and B_L under different confining pressures was derived from the data in Table 3 and plotted as Figure 7. As shown in the figure, B_L correctly reflected the brittle abnormalities for the specimen at 15MPa, which is better than B_{12}, and declined with the growth in confining pressure. Therefore, B_L is an ideal index to identify the anomalies of specimen brittleness at 15MPa.

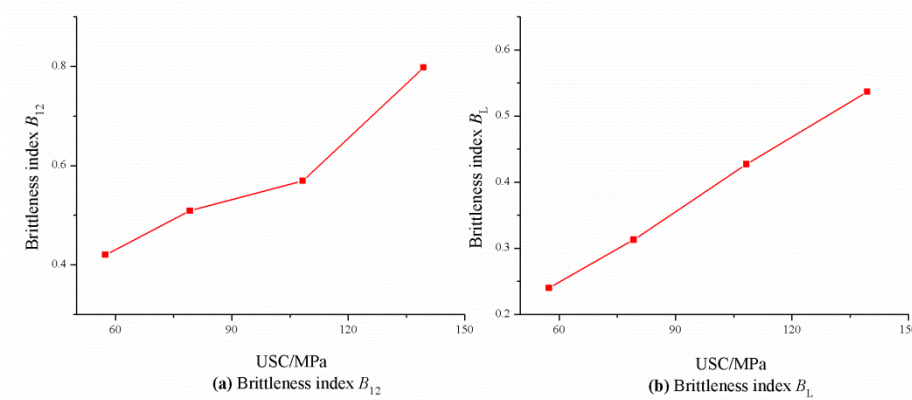### *4.2. Further validation of B_L under uniaxial compression*

Figure 8. B_{12} and B_L under uniaxial compression

The variation in B_{12} and B_L under uniaxial compression was derived from the data in Table 4 and plotted as Figure 8. As shown in the figure, B_L increased with the uniaxial load, and the correlation was more obvious than B_{12}. This trend agrees well with the experimental data, indicating that B_L can accurately identify the anomalies of specimen brittleness at 15MPa. Overall, B_L is a desirable tool to evaluate rock brittleness under uniaxial compression.

5. Conclusions

Considering the importance of brittleness evaluation in rock engineering, this paper proposes a new index B_L to evaluate rock brittleness and validates it through tests under uniaxial compression and different confining pressures. The accuracy and feasibility of the index were verified against the experimental results. Through the research, the following conclusions were derived:

(1) Based on the drop rate ratio and peak strength, the proposed index could accurately identify rock brittleness under different confining pressures, and outperform other indices like B_8, B_{11} and B_{12} in revealing the variation of rock brittleness.

(2) The index B_L could accurately reflect the brittle anomalies of the rock specimen at the confining pressure of 15MPa, making it a desirable tool to evaluate rock brittleness under uniaxial compression.

References

Akrad O., Miskimins J. L., Prasad M. (2012). The impact of mechanical stratigraphy on hydraulic fracture growth and design considerations for horizontal wells. *Bulletin*, Vol. 91, No. 4, pp. 475-499.

Altindag R. (2002). The evaluation of rock brittleness concept on rotary blast hold drills. *Journal of the Southern African Institute of Mining and Metallurgy*, Vol. 102, No. 1, pp. 61-66.

Bai M. (2016). Why are brittleness and fracability not equivalent in designing hydraulic fracturing in tight shale gas reservoirs. *Petroleum*, Vol. 2, No. 1, pp. 1-19. https://doi.org/10.1016/j.petlm.2016.01.001

Bishop A. W. (1967). Progressive failure with special reference to the mechanism causing it. *Proceedings of Geotechnical Conference, Oslo, Norway*, Vol. 2, pp. 142-150.

Dursun A. E., Gokay M. K. (2016). Cuttability assessment of selected rocks through different brittleness values. *Rock Mechanics and Rock Engineering*, Vol. 49, No. 4, pp. 1173-1190. https://doi.org/10.1007/s00603-015-0810-2

El-Ebrashi M. K., Craig R. G., Peyton F. A. (1969). Experimental stress analysis of dental restorations. Part III. The concept of the geometry of proximal margins. *Journal of Prosthetic Dentistry,* Vol. 22, No. 3, pp. 333-345. https://doi.org/10.1016/0022-3913(69)90195-4

Gong Q. M., Zhao J. (2007). Influence of rock brittleness on TBM penetration rate in Singapore granite. *Tunnelling and Underground Space Technology*, Vol. 22, No. 3, pp. 317-324. https://doi.org/10.1016/j.tust.2006.07.004

Hajiabdolmajid V., Kaiser P. (2003). Brittleness of rock and stability assessment in hard rock tunneling. *Tunnelling and Underground Space Technology*, Vol. 18, No. 1, pp. 35-48. https://doi.org/10.1016/S0886-7798(02)00100-1

Holt R. M., Fjær E., Stenebråten J. F., Nes O. M. (2015). Brittleness of shales: relevance to borehole collapse and hydraulic fracturing. *Journal of Petroleum Science and Engineering*, Vol. 131, pp. 200-209. https://doi.org/10.1016/j.petrol.2015.04.006

Hucka V., Das B. (1974). Brittleness determination of rocks by different methods. International *Journal of Rock Mechanics and Mining Sciences & Geomechanics Abstracts*, Vol. 11, No. 10, pp. 389-392. https://doi.org/10.1016/0148-9062(74)91109-7

Kahraman S. (2002). Correlation of TBM and drilling machine performances with rock brittleness. *Engineering Geology*, Vol. 65, No. 4, pp. 269-283. https://doi.org/10.1016/S0013-7952(01)00137-5

Kahraman S., Altindag R. (2004). A brittleness index to estimate fracture toughness. *International Journal of Rock Mechanics and Mining Sciences*, Vol. 41, No. 2, pp. 343-348. https://doi.org/10.1016/j.ijrmms.2003.07.010

Lawn B. R., Marshall D. B. (1979). Hardness, toughness, and brittleness: an indentation analysis. *Journal of the American ceramic society*, Vol. 62, No. 7-8, pp. 347-350. https://doi.org/10.1111/j.1151-2916.1979.tb19075.x

Lee K. H., Lee I. M., Shin Y. J. (2012). Brittle rock property and damage index assessment for predicting brittle failure in excavations. *Rock Mechanics and Rock Engineering*, Vol. 45, No. 2, pp. 251-257. https://doi.org/10.1007/s00603-011-0189-7

Liu Z. S., Sun Z. D. (2015). New brittleness indexes and their application in shale/clay gas reservoir prediction. *Petroleum Exploration and Development*, Vol. 42, No. 1, pp. 129-137. https://doi.org/10.1016/S1876-3804(15)60016-7

Meng F. Z., Zhou H., Zhang C. Q., Xu R. C., Lu J. J. (2015). Evaluation methodology of brittleness of rock based on post-peak stress–strain curves. *Rock Mechanics and Rock Engineering*, Vol. 48, No. 5, pp. 1787-1805. https://doi.org/10.1007/s00603-014-0694-6

Morley A. (1944). Strength of Material, Longman, Green, London.

Nygård R., Yenice H., Şimşir F., Yaralı O. (2006). Brittle–ductile transition, shear failure and leakage in shales and mudrocks. *Marine and Petroleum Geology,* Vol. 23, No. 2, pp. 201-212. https://doi.org/10.1016/j.marpetgeo.2005.10.001

Obert L., Duvall W. I. (1967). Rock mechanics and the design of structures in rock. *New York, J. Wiley*.

Özfırat M. K., Yenice H., Şimşir F., Yaralı O. (2016). A new approach to rock brittleness and its usability at prediction of drillability. *Journal of African Earth Sciences*, Vol. 119, pp. 94-101. https://doi.org/10.1016/j.jafrearsci.2016.03.017

Qinghui L., Mian C., Yan J., Bing H., Bao-wei Z. (2012). Indoor evaluation method for shale brittleness and improvement. *Chinese Journal of Rock Mechanics and Engineering*, Vol. 31, No. 8, pp. 1680-1685.

Quinn J. B., Quinn G. D. (1997). Indentation brittleness of ceramics: a fresh approach. *Journal of Materials Science*, Vol. 32, No. 16, pp. 4331-4346. https://doi.org/10.1023/A:1018671823059

Ramsay J. (1967). Folding and fracturing of rocks.

Rickman R., Mullen M. J., Petre J. E., Grieser W. V., Kundert D. (2008). A practical use of shale petrophysics for stimulation design optimization: all shale plays are not clones of the barnett shale. *SPE Annual Technical Conference and Exhibition*. https://doi.org/10.2118/115258-MS

Tarasov B. G., Potvin Y. (2012). Absolute, relative and intrinsic rock brittleness at compression. *Mining Technology*, Vol. 121 No. 4, pp. 218-225. https://doi.org/10.1179/1743286312Y.0000000015

Tarasov B., Potvin Y. (2013). Universal criteria for rock brittleness estimation under triaxial compression. *International Journal of Rock Mechanics and Mining Sciences*, Vol. 59, pp. 57-69. https://doi.org/10.1016/j.ijrmms.2012.12.011

Yagiz S. (2009). Assessment of brittleness using rock strength and density with punch penetration test. *Tunnelling and Underground Space Technology*, Vol. 24, No. 1, pp. 66-74. https://doi.org/10.1016/j.tust.2008.04.002

Yarali O., Kahraman S. (2011). The drillability assessment of rocks using the different brittleness values. *Tunnelling and Underground Space Technology*, Vol. 26, No. 2, pp. 406-414. https://doi.org/10.1016/j.tust.2010.11.013

Zhao Z. M., Esamaldeen A., Wu G., Wang X. H. (2015). Assessment of strain energy storage and rock brittleness indices of rockburst potential from microfabric characterizations. *American Journal of Earth Sciences*, Vol. 2, No. 1, pp. 8-14.